# On Haney-Type Surface Thermal Boundary Conditions for Ocean Circulation Models

PETER C. CHU, YUCHUN CHEN, AND SHIHUA LU

*Department of Oceanography, Naval Postgraduate School, Monterey, California*

(Manuscript received 5 December 1996, in final form 14 August 1997)

ABSTRACT

Haney-type surface thermal boundary conditions linearly connect net downward surface heat flux $Q$ to air–sea temperature difference (gradient-type condition) $\Delta T_1$ or to climate/synoptic sea temperature difference (restoring-type condition) $\Delta T_2$ by a coupling coefficient $\kappa$. In this study, the authors used the global reanalyzed data (6-h resolution) of $Q$, surface air temperature $T_A$, and sea surface temperature $T_O$ from the National Centers for Environmental Prediction during 1 October 1994–31 December 1995 to verify the validity of Haney-type surface thermal boundary conditions. First, daily means of these variables were computed to get rid of diurnal variation. Second, the cross-correlation coefficients (CCC) between $Q$ and ($\Delta T_1$, $\Delta T_2$) were calculated. The ensemble mean CCC fields show (i) no correlation between $Q$ and $\Delta T_2$ anywhere in the world oceans, (ii) no correlation between $Q$ and $\Delta T_1$ in the equatorial regions, and (c) evident correlation (CCC $\geq$ 0.7) between $Q$ and $\Delta T_1$ in the middle and high latitudes. Third, the variance analysis was conducted and a value of 70 W m$^{-2}$ K$^{-1}$ (65 W m$^{-2}$ K$^{-1}$) was suggested for the coupling coefficient $\kappa$ in the northern (southern) middle and high latitude zone.

Thus, the authors find that the restoring-type surface thermal conditions by no means represent the net air–ocean heat flux anywhere in the world oceans. However, the gradient-type surface thermal condition represents the net heat flux quite well for the middle and high latitudes. In addition, it is also found that, if the solar shortwave component is treated separately, the gradient-type condition will have more fidelity for the middle and high latitudes.

## 1. Introduction

The ocean is thermally driven by the net downward flux of heat across the ocean surface, $Q$, which is the sum of the downward flux of solar radiation, $R_S$, minus the net upward flux of longwave (or ''back'' radiation) $R_b$, sensible heat $Q_H$, and latent heat $Q_E$,

$$Q = R_S - (R_b + Q_H + Q_E). \tag{1}$$

Under the assumption that the ocean is in contact with an atmospheric equilibrium state (i.e., an atmosphere with a near-infinite heat capacity), Haney (1971) obtained a very simple heat flux formulation,

$$Q = \kappa \Delta T, \qquad \Delta T = T_A^* - T_O, \tag{2}$$

where $T_A^*$ is the apparent atmospheric equilibrium temperature, $T_O$ the sea surface temperature (SST), and $\kappa$ is a coupling coefficient. In spite of its temporal variation, the parameter is usually taken as positive values between 10 and 50 W m$^{-2}$ K$^{-1}$ by various authors (e.g., Marotzke 1994; Cai and Chu 1996). Here $T_A^*$ should be computed from surface heat fluxes and their dependence on temperature, as done by Han (1984) and Oberhuber (1988). Despite Haney's emphasis that $Q$ is proportional to $T_A^* - T_O$, many subsequent investigators have replaced $T_A^*$ by $T_A$ or $T_O^*$. Here $T_A$ is the surface air temperature (SAT), and $T_O^*$ is either the climatological mean $\langle T_O \rangle$ or observed SST. In this paper, we verify the case where $T_O^* = \langle T_O \rangle$. Thus, the Haney condition becomes

$$Q = \kappa \Delta T_1, \qquad \Delta T_1 = T_A - T_O, \tag{3}$$

which is the gradient-type condition, and

$$Q = \kappa \Delta T_2, \qquad \Delta T_2 = \langle T_O \rangle - T_O, \tag{4}$$

which is the restoring-type condition. Pierce (1996) pointed out two distinct disadvantages of the restoring-type conditions: (i) it imposes a time lag in the model's surface tracer field and (ii) it systematically underrepresents the model's surface variability. Under the assumption that the surface fluxes contribute more to SST changes than do internal ocean processes, Pierce proposed a method to correct the amplitude and phase of $T_O$ for (4).

Another trend is to separate the solar radiation from the net downward flux (e.g., Blumberg and Mellor 1987)

$$Q = R_S + \tilde{Q}, \qquad \tilde{Q} \equiv -(R_b + Q_H + Q_E) \tag{5}$$

and to replace $Q$ by $\tilde{Q}$ in the gradient-type surface boundary condition

$$\tilde{Q} = \kappa \Delta T_1 \tag{6}$$

*Corresponding author address:* Prof. Peter C. Chu, Department of Oceanography, Naval Postgraduate School, Monterey, CA 93943-5000.
E-mail: chu@nps.navy.mil

and the restoring-type surface boundary condition

$$\tilde{Q} = \kappa \Delta T_2. \tag{7}$$

We call $Q$ the net downward heat flux with solar radiation, and $\tilde{Q}$ the downward heat flux without solar radiation.

Since the Haney-type boundary conditions have been used by the community for more than two decades, it is time to verify the validity of these conditions. How good are these conditions? Is there any temporal and spatial variation of the validity of these conditions?

## 2. Statistical evaluation

### a. Dataset

We chose the National Centers for Environmental Prediction (NCEP) reanalyzed global surface fluxes $R_S$, $R_b$, $Q_H$, $Q_E$, and temperatures $T_O$ (skin temperature), $T_A$ data on a 1.875° × 1.875° grid for this study. The temporal resolution of the original data is 6 h. Since Haney-type surface thermal boundary conditions are commonly used for ocean modeling on a seasonal timescale or longer, we first computed daily means of these variables to filter out diurnal variation and to obtain a dataset of global $Q(x, y, d)$, $\tilde{Q}(x, y, d)$, $T_A(x, y, d)$, $T_O(x, y, d)$ for each day, $d$, from 1 October 1994 to 31 December 1995. Then, from $T_O(x, y, d)$ data, we computed the monthly mean values $\langle T_O \rangle$ at each grid.

### b. Cross-correlation coefficient

The validity of Haney-type boundary conditions (3), (4), (6), and (7) should be first tested by cross-correlation coefficients (CCC) between the two time series: $Q$ [$Q$ or $\tilde{Q}$] and $\Delta T$ [$\Delta T_1$ or $\Delta T_2$] at day $d$, which is computed in this paper from a 91-day subset between 45 days prior to and 45 days after that date,

$$R_{Q,\Delta T}(d) = \frac{\frac{1}{N}\sum_{i=1}^{N} \{[Q(x, y, \tau_i) - \overline{Q}(x, y)][\Delta T(x, y, \tau_i) - \overline{\Delta T}(x, y)]\}}{\sigma_Q(d)\sigma_{\Delta T}(d)} \qquad (d - 45 \le \tau_i \le d + 45), \tag{8}$$

where $N = 91$ days, $(x, y)$ the horizontal coordinates, $\overline{Q}(x, y)$ and $\overline{\Delta T}(x, y)$ the temporal means of the subset data,

$$\overline{Q}(x, y) = \frac{1}{N}\sum_{i=1}^{N} Q(x, y, \tau_i),$$

$$\overline{\Delta T}(x, y) = \frac{1}{N}\sum_{i=1}^{N} \Delta T(x, y, \tau_i), \tag{9}$$

and $\sigma_Q(d)$ and $\sigma_{\Delta T}(d)$ the standard deviations of the subset data,

$$\sigma_Q(d) = \sqrt{\frac{1}{N-1}\sum_{i=1}^{N} [Q(x, y, \tau) - \overline{Q}(x, y)]^2}$$

$$\sigma_{\Delta T}(d) = \sqrt{\frac{1}{N-1}\sum_{i=1}^{N} [\Delta T(x, y, \tau_i) - \overline{\Delta T}(x, y)]^2}. \tag{10}$$

Thus, we established little over one year (368 days: 16 November 1994–18 November 1995) four CCC datasets: $R_{Q,\Delta T_1}$, $R_{\tilde{Q},\Delta T_1}$, $R_{Q,\Delta T_2}$, and $R_{\tilde{Q},\Delta T_2}$. The higher the values of CCC, the higher the confidence of a linear relationship between $(Q, \tilde{Q})$ and $(\Delta T_1, \Delta T_2)$.

Besides the correlation analysis, we still need to do the variance analysis, because it does matter if $(Q, \tilde{Q})$ and $(\Delta T_1, \Delta T_2)$ correlate closely, but typically used values of $\kappa$ (10–50 W m$^{-2}$ K$^{-1}$) end up missing all the variance.

### c. Determination of $\kappa$ by no-missing variance

Since the value of $\kappa$ is quite uncertain, such a variance comparison between $(Q, \tilde{Q})$ and $(\Delta T_1, \Delta T_2)$ depends on the choice of $\kappa$. On the other hand, we may determine the value of $\kappa$ by no-missing variance

$$\kappa(d) = \frac{\sigma_Q(d)}{\sigma_{\Delta T}(d)} R_{Q,\Delta T} \tag{11}$$

and check if the values are within a reasonable range.

## 3. Statistical tests

Whether the sample values of $R_{Q,\Delta T}$ represent good or bad linear relationships (3), (4), (6), and (7) between $(Q, \tilde{Q})$ and $(\Delta T_1, \Delta T_2)$ should be tested. First, we use the $t$ test to identify the region with small values of CCC in which there is no correlation between $(Q, \tilde{Q})$ and $(\Delta T_1, \Delta T_2)$. Second, we set up a prior significant value $(\rho_0)$ for CCC, and use the $z$ test to see where the values of $R_{Q,\Delta T}$ are significantly larger than $\rho_0$.

### a. No correlation between Q and ΔT (t test)

The $t$ value for any location $(x, y)$, computed by

$$t = \frac{R_{Q,\Delta T}\sqrt{N-2}}{\sqrt{1 - R_{Q,\Delta t}}}, \tag{12}$$

is used to assess the statistical significance of $R_{Q,\Delta T}$ dif-

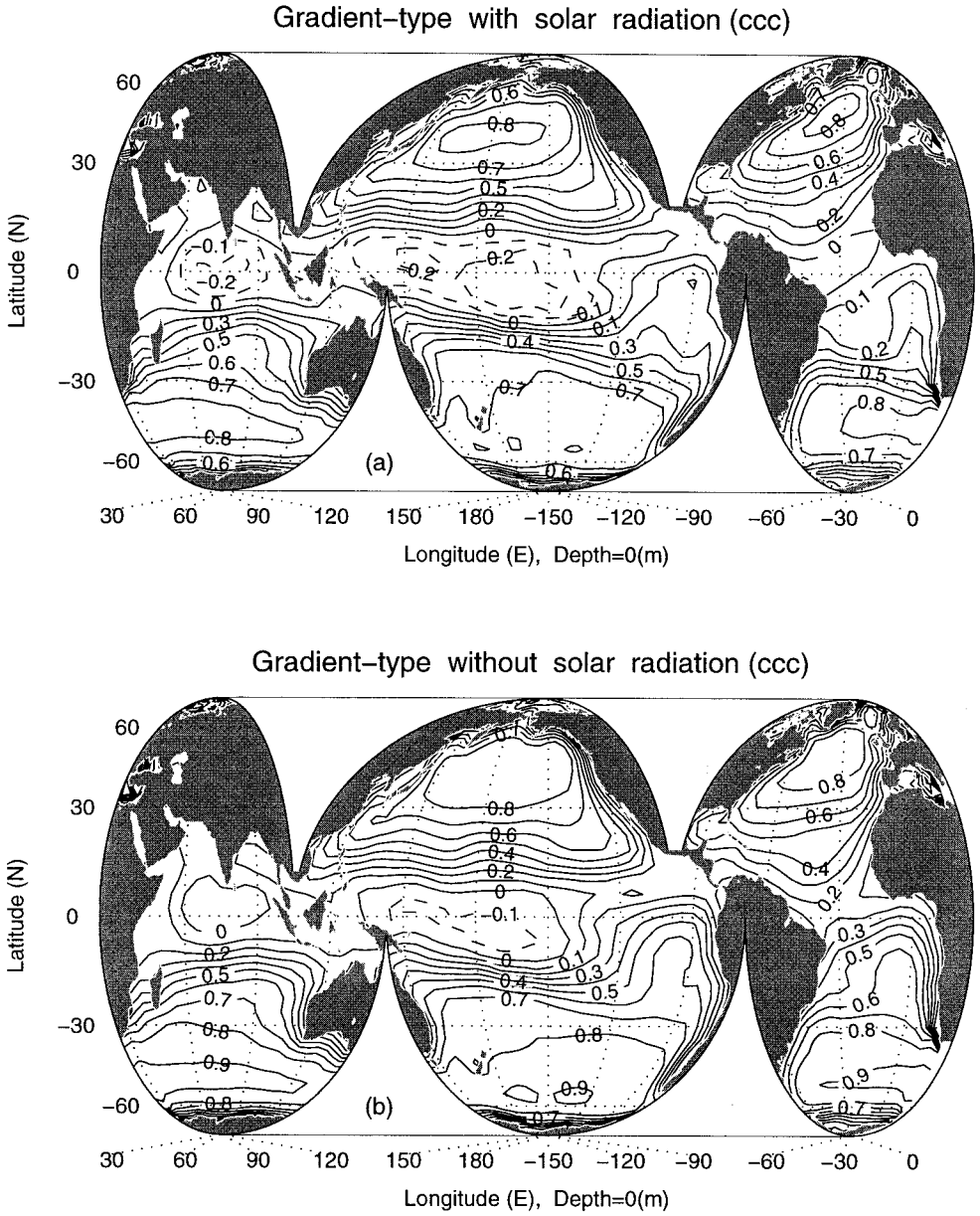


FIG. 1. Ensemble mean cross-correlation coefficients between $\Delta T_1$ and net surface heat flux: (a) with solar radiation $Q$, (b) without solar radiation $\tilde{Q}$, and (c) correlation coefficient ($\times 100$) between monthly anomalous latent and sensible heat flux and changes in SST anomalies (Fig. 1c from Cayan 1992).

ferent from 0. We begin with the null hypothesis that the two variables $Q$ and $\Delta T$ are not positively correlated. The significance level $\alpha$ is the probability that the given value of $t$ is exceeded purely by chance. Equivalently, it is the probability of incorrectly rejecting the null hypothesis. For a given significance level $\alpha$ ($\alpha = 0.05$ was used), we compare the $t$ value with $t_\alpha$: if $t < t_\alpha$, we accept the null hypothesis, and there is no linear (positive) relationship between $Q$ and $\Delta T$ at the given location $(x, y)$.

*b. Significant correlation ($R_{Q,\Delta T} > \rho_0$) between Q and ΔT (z test)*

The $z$ value, computed by

$$z = \frac{\sqrt{N-3}}{2} \ln\left[\frac{(1 + R_{Q,\Delta T})(1 - \rho_0)}{(1 - R_{Q,\Delta T})(1 + \rho_0)}\right], \quad (13)$$

is used to assess the statistical significance of

$$R_{Q,\Delta T} > \rho_0 \quad (14)$$

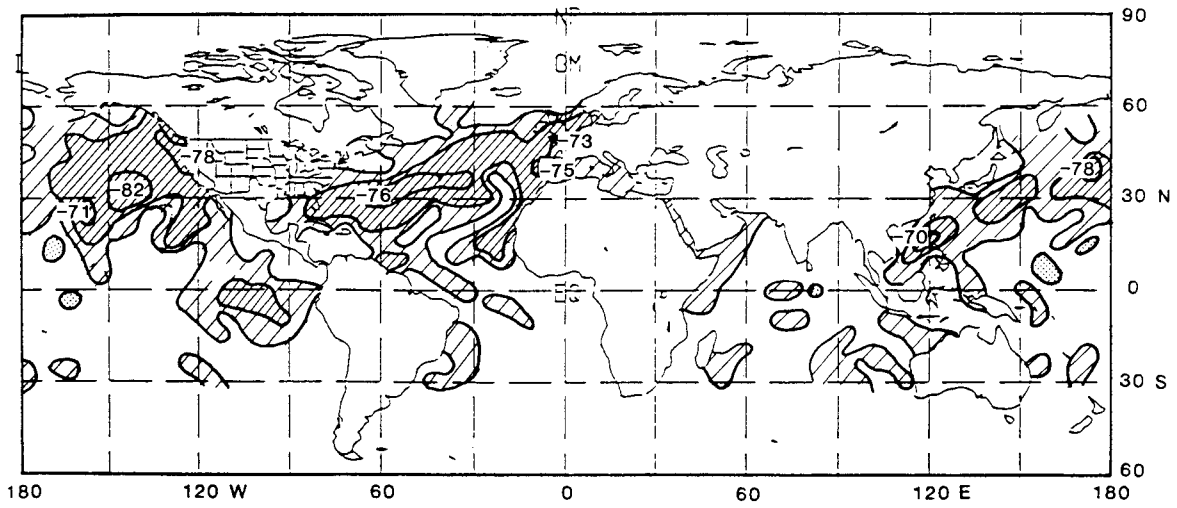


FIG. 1. (*Continued*)

for any location $(x, y)$. This $z$ value satisfies the normal distribution.

We start with the null hypothesis that $H_0$: $R_{Q,\Delta T} = \rho_0$, $H_1$: $R_{Q,\Delta T} > \rho_0$. The significance level $\alpha$ is the probability that the given value of $z$ is exceeded purely by chance. For a given significance level $\alpha$ ($\alpha = 0.05$ was used), we compare the $z$ value with $z_\alpha$: if $z > z_\alpha$, we accept $H_1$, and the CCC between $Q$ and $\Delta T$ exceeds $\rho_0$ at the given location $(x, y)$. In this study, we use $\rho_0 = 0.7$.

After $R_{Q,\Delta T_1}(x, y, d)$, $R_{\tilde{Q},\Delta T_1}(x, y, d)$, $R_{Q,\Delta T_2}(x, y, d)$, and $R_{\tilde{Q},\Delta T_2}(x, y, d)$ are calculated, we used (12) to compute $t$ values and (13) to calculate the $z$ values for each grid point, compared the $t$ values to $t_\alpha$ to test if $(Q, \tilde{Q})$ and $(\Delta T_1, \Delta T_2)$ were independent, and compared the $z$ values to $z_\alpha$ to test if $R_{Q,\Delta T_1}(x, y, d)$, $R_{\tilde{Q},\Delta T_1}(x, y, d)$, $R_{Q,\Delta T_2}(x, y, d)$, and $R_{\tilde{Q},\Delta T_2}(x, y, d)$ were significant.

## 4. CCC fields over the world oceans

Four time series, $R_{Q,\Delta T_1}(x, y, d)$, $R_{\tilde{Q},\Delta T_1}(x, y, d)$, $R_{Q,\Delta T_2}(x, y, d)$, and $R_{\tilde{Q},\Delta T_2}(x, y, d)$, were decomposed into ensemble means:

$$\langle R_{Q,\Delta T_1}\rangle = \frac{1}{368}\sum_d R_{Q,\Delta T_1}(x, y, d),$$

$$\langle R_{\tilde{Q},\Delta T_1}\rangle = \frac{1}{368}\sum_d R_{\tilde{Q},\Delta T_1}(x, y, d),$$

$$\langle R_{Q,\Delta T_2}\rangle = \frac{1}{368}\sum_d R_{Q,\Delta T_2}(x, y, d),$$

$$\langle R_{\tilde{Q},\Delta T_2}\rangle = \frac{1}{368}\sum_d R_{\tilde{Q},\Delta T_2}(x, y, d), \qquad (15)$$

which show the overall linear relationships between $(Q, \tilde{Q})$ and $(\Delta T_1, \Delta T_2)$ and anomalies:

$$R'_{Q,\Delta T_1} = R_{Q,\Delta T_1} - \langle R_{Q,\Delta T_1}\rangle,$$

$$R'_{\tilde{Q},\Delta T_1} = R_{\tilde{Q},\Delta T_1} - \langle R_{\tilde{Q},\Delta T_1}\rangle,$$

$$R'_{\tilde{Q},\Delta T_2} = R_{Q,\Delta T_2} - \langle R_{Q,\Delta T_2}\rangle,$$

$$R'_{\tilde{Q},\Delta T_2} = R_{\tilde{Q},\Delta T_2} - \langle R_{\tilde{Q},\Delta T_2}\rangle, \qquad (16)$$

which indicate temporal variations of such relationships.

### a. Ensemble mean CCC fields

#### 1) GRADIENT-TYPE CONDITIONS

Figures 1a and 1b illustrate the global distributions of $\langle R_{Q,\Delta T_1}\rangle$ and $\langle R_{\tilde{Q},\Delta T_1}\rangle$, respectively. The region with large values ($\geq$0.7) of $\langle R_{Q,\Delta T_1}\rangle$ (or $\langle R_{\tilde{Q},\Delta T_1}\rangle$) is called the valid region, and the region with small values ($\leq$0.2) of $\langle R_{Q,\Delta T_1}\rangle$ (or $\langle R_{\tilde{Q},\Delta T_1}\rangle$) is called the invalid region. The gradient-type Haney boundary conditions with and without solar radiation are valid in middle and high latitudes (higher than 30°) away from coasts, and are invalid in equatorial regions (10°N–10°S). The invalidity in the equatorial and coastal regions may imply the improper representation of latent heat $Q_E$ by temperature difference $\Delta T_1$.

Under the assumption that the upper ocean is a constant-depth well-mixed slab that exchanges heat with the atmosphere, Cayan (1992) computed CCC (Fig. 1c) between monthly anomalous latent and sensible heat flux and changes in SST anomalies over the North Atlantic and North Pacific from the monthly summaries trimmed subset of the Comprehensive Ocean–Atmosphere Data Set (COADS). Comparison of Fig. 1a and 1b with Fig. 1c shows a substantial agreement (high CCC in middle and high latitudes and low CCC in equatorial regions).

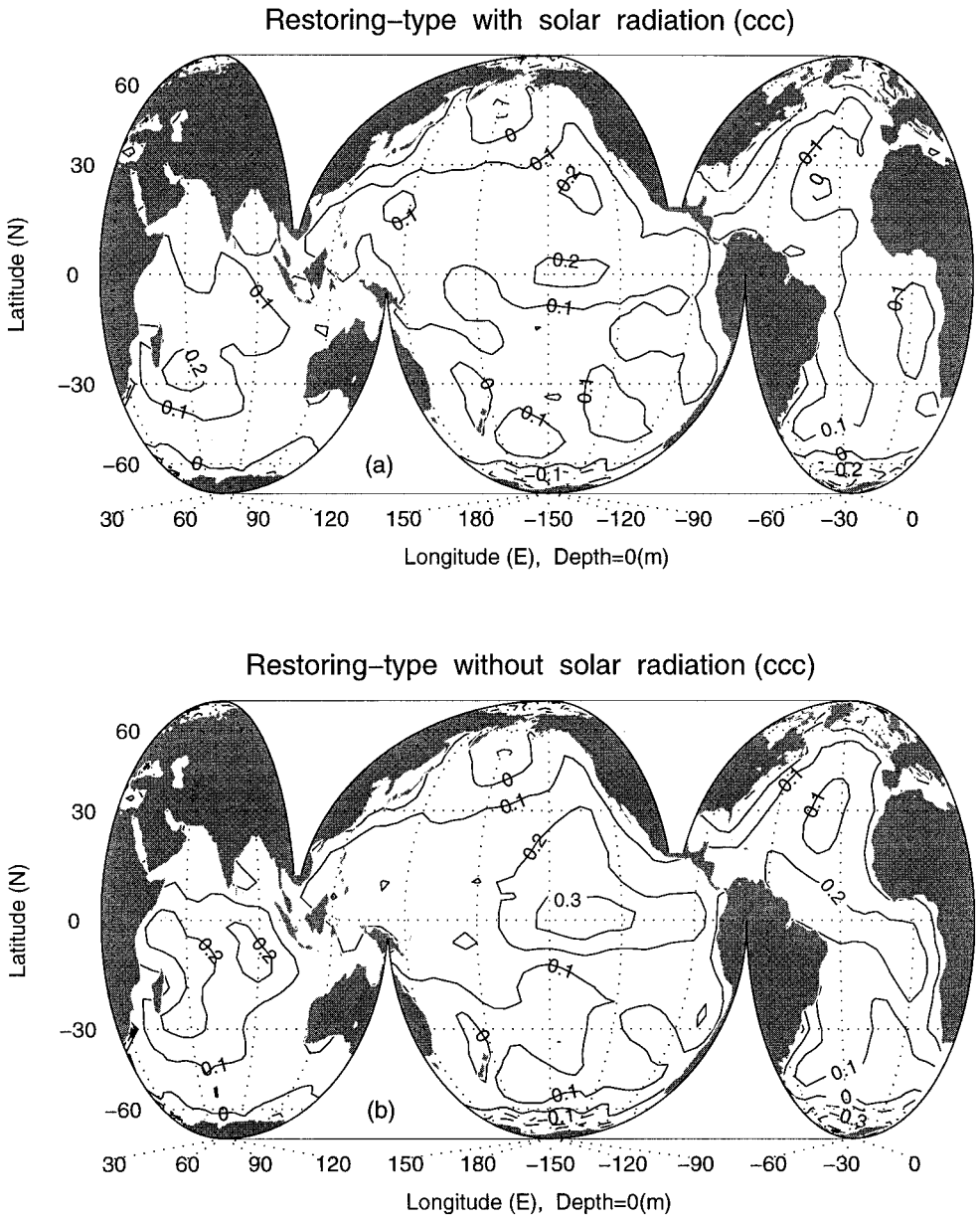


FIG. 2. Ensemble mean cross-correlation coefficients between $\Delta T_2$ and net surface heat flux (a) with solar radiation $Q$ and (b) without solar radiation $\tilde{Q}$.

2) RESTORING-TYPE CONDITIONS

Figure 2 illustrates the global distributions of $\langle R_{Q,\Delta T_2}\rangle$ and $\langle R_{\tilde{Q},\Delta T_2}\rangle$, respectively. The small values (less than 0.2) of $\langle R_{Q,\Delta T_2}\rangle$ and $\langle R_{\tilde{Q},\Delta T_2}\rangle$ are all over the globe except the eastern equatorial Pacific and South Atlantic section near Antarctica, where $\langle R_{\tilde{Q},\Delta T_2}\rangle$ has values around 0.3. No correlation between ($Q$, $\tilde{Q}$) and $\Delta T_2$ may indicate that the restoring-type surface thermal condition by no means represents the net air–ocean heat flux anywhere in the world oceans.

*b. Anomaly CCC fields*

We used empirical orthogonal function (EOF) analysis to delineate the major modes of variability of the anomaly CCC fields: $R'_{Q,\Delta T_1}$ and $R'_{Q,\Delta T_2}$, which are decomposed by

$$R' = \sum_{\alpha} \mathrm{PC}_{\alpha}(d)\phi_{\alpha}(x_i, y_j), \tag{17}$$

where $\mathrm{PC}_{\alpha}(d)$ is the principal component, representing the temporal variation of the associated spatial pattern described by EOF $\phi_{\alpha}(x_i, y_j)$. The time series is anal-

TABLE 1. Variances of the first six leading EOFs for the gradient-type conditions.

| EOF | With solar radiation | Without solar radiation |
|---|---|---|
| 1 | 0.643 | 0.742 |
| 2 | 0.179 | 0.158 |
| 3 | 0.073 | 0.040 |
| 4 | 0.038 | 0.020 |
| 5 | 0.017 | 0.009 |
| 6 | 0.012 | 0.009 |

ogous to a projection of CCC anomaly through the ''filter'' of an EOF mode during a timescale.

The first two leading EOFs are able to account for 82% (for $R'_{Q,\Delta T_1}$) and 90% (for $R'_{Q,\Delta T_2}$) of the total variance during the period (Table 1). Each EOF mode is normalized so that its spatial variance is equal to unity. So, the patterns of the first two EOFs are enough to explain the spatial anomalies of the global CCCs. Here, we show only EOF1 and $PC_1$ for $R$ as an example.

The EOF1 mode (Fig. 3a) has a dipole pattern featuring the Northern Hemisphere positive (maximum value near 0.02) and Southern Hemisphere negative (minimum value near $-0.02$), and accounts for up to 64.3% of the total spatial variance. This pattern is believed to be related to the solar radiation. The first principal component, $PC_1(d)$, during the integration period is shown in Fig. 3b. EOF1 mode $\phi_1(x_i, y_j)$ is generally positive (negative) in the Northern (Southern) Hemisphere (Fig. 3a). Therefore, $PC_1(d) > 0$ corresponds to positive (negative) CCC anomalies in the Northern (Southern) Hemisphere, and $PC_1(d) < 0$ corresponds to negative (positive) CCC anomalies in the Northern (Southern) Hemisphere. Figure 3b shows a strong seasonal variation: From late October, when $PC_1(d) = 0$, it increases with time until mid-January when $PC_1$ reaches the maximum value of 9.0, and then decreases to 0 in early March. After early March, $PC_1$ becomes negative until late October and reaches the minimum value of $-7.0$ in early July. From late October to early March, the Northern (Southern) Hemisphere is winter (summer); $PC_1(d) > 0$. The contribution of EOF1 to the total CCC field,

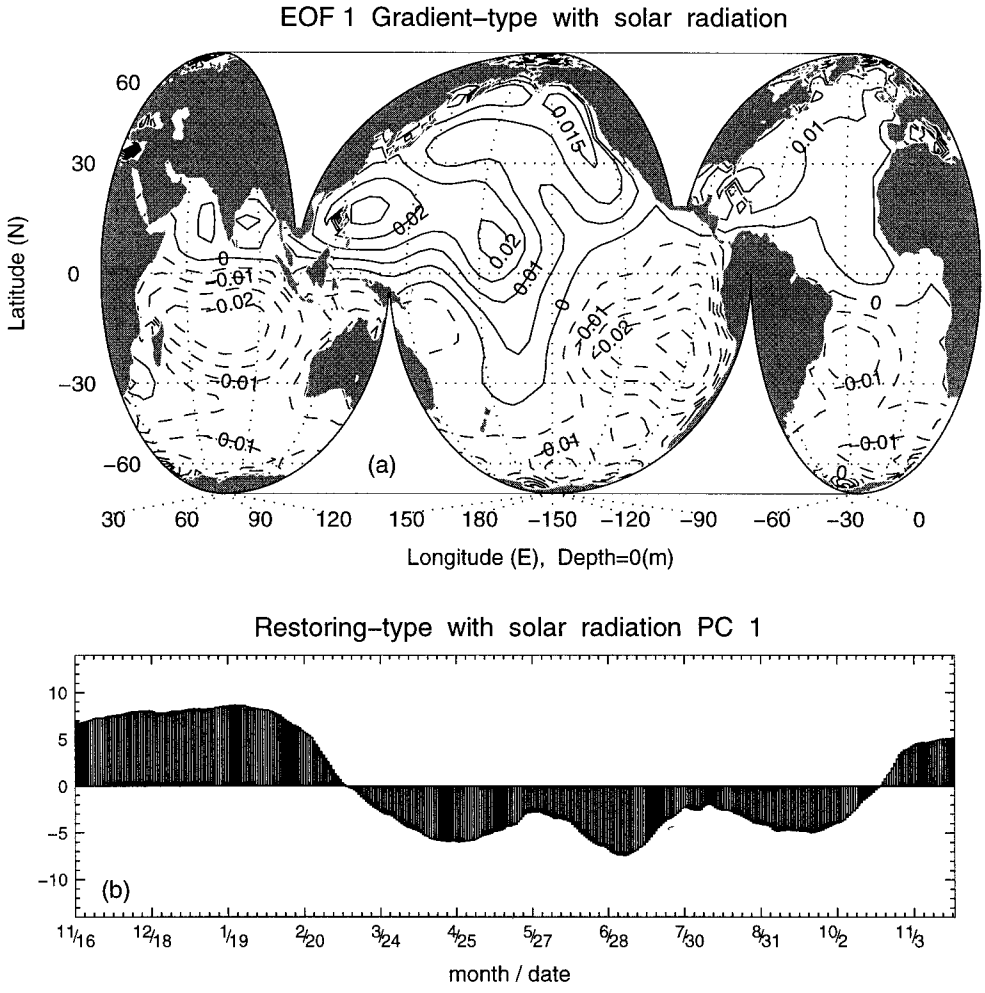


FIG. 3. (a) First EOF mode of $R'_{Q,\Delta T_1}$ and (b) associated time series of $PC_1$.

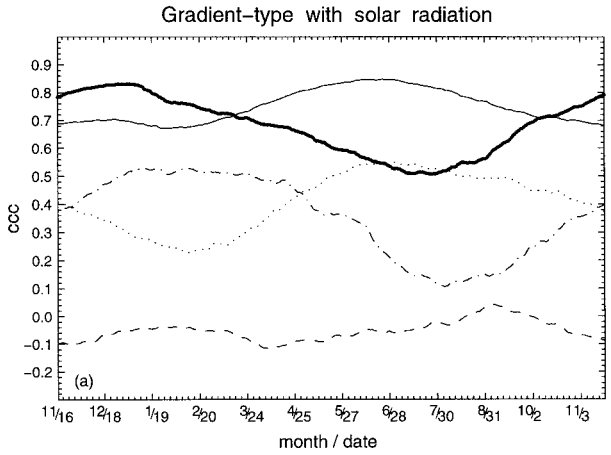


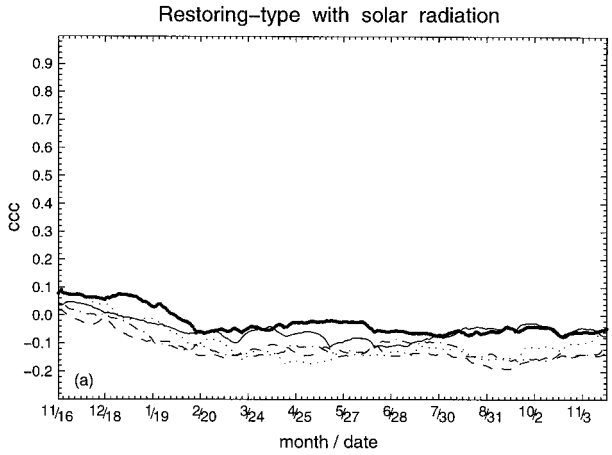


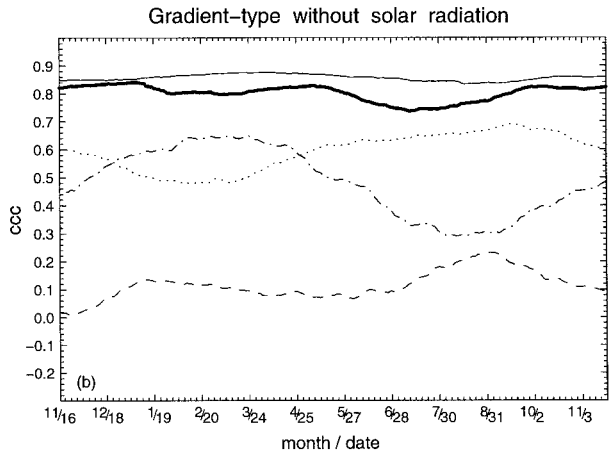


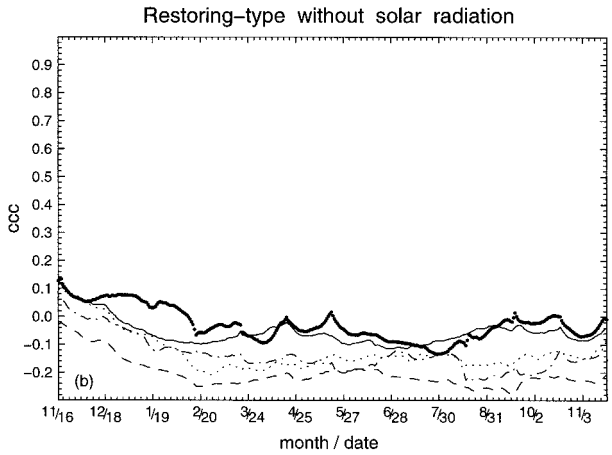


FIG. 4. Seasonal variation of cross-correlation coefficients averaged within five geographic zones between (a) $Q$ and $\Delta T_1$ and (b) $\tilde{Q}$ and $\Delta T_1$. Here the thin solid curve indicates the southern middle and high latitude zone (south to 30°S), the thick solid curve indicates the northern middle and high latitude zone (north to 30°N), the dotted curve indicates the southern subtropical zone (10°–30°S), the dashed–dotted curve indicates the northern subtropical zone (10°–30°N), and the dashed curve indicates the equatorial zone (10°S–10°N).

FIG. 5. Seasonal variation of cross-correlation coefficients averaged within five geographic zones between (a) $Q$ and $\Delta T_2$ and (b) $\tilde{Q}$ and $\Delta T_2$. Here the thin solid curve indicates the southern middle and high latitude zone (south to 30°S), the thick solid curve indicates the northern middle and high latitude zone (north to 30°N), the dotted curve indicates the southern subtropical zone (10°–30°S), the dashed–dotted curve indicates the northern subtropical zone (10°–30°N), and the dashed curve indicates the equatorial zone (10°S–10°N).

$\mathrm{PC}_1(d) \times \phi_1(x_i, y_j)$, adds positive values to the ensemble CCCs with a maximum increasing value of 0.18 ($=9.0 \times 0.02$) in the Northern Hemisphere and adds negative values to the ensemble CCCs with a maximum decreasing value of $-0.18$ [$=9.0 \times (-0.02)$] in the Southern Hemisphere. On the other hand, from early March to late October $\mathrm{PC}_1(d) < 0$. The contribution of EOF1 to the total CCC field is reversed to the period from late October to early March. Thus, the winter hemisphere has better cross correlations than the summer hemisphere. The maximum temporal variability can reach 0.36 ($=2 \times 0.18$). This is because the surface solar radiation cannot be well represented by the temperature difference $\Delta T_1$.

## 5. Seasonal CCC variation in five geographic zones

On the basis of the spatial variation of the ensemble mean field, we divided the world oceans into five geographic zones: equatorial zone (10°N–10°S), northern subtropical zone (10°–30°N), southern subtropical zone (10°–30°S), northern middle and high latitude zone (north of 30°N), and southern middle and high latitude zone (south of 30°S). At each day, we averaged the CCC data $R_{Q,\Delta T_1}(x, y, d)$, $R_{\tilde{Q},\Delta T_1}(x, y, d)$, $R_{Q,\Delta T_2}(x, y, d)$, and $R_{\tilde{Q},\Delta T_2}(x, y, d)$ spatially within each zone. Thus, we obtained five time series for each of the CCC data: $\overline{R}^S_{Q,\Delta T_1}(d)$, $\overline{R}^S_{\tilde{Q},\Delta T_1}(d)$, $\overline{R}^S_{Q,\Delta T_2}(d)$, $\overline{R}^S_{\tilde{Q},\Delta T_2}(d)$. Here, the superscript "$S$" means the spatial average.

### a. Gradient-type conditions

#### 1) WITH SOLAR RADIATION

Figure 4a illustrates the seasonal variation of $\overline{R}^S_{Q,\Delta T_1}(d)$ for the five geographic zones. The value fluctuates from $-0.1$ to 0.05 in the equatorial zone (no correlation be-

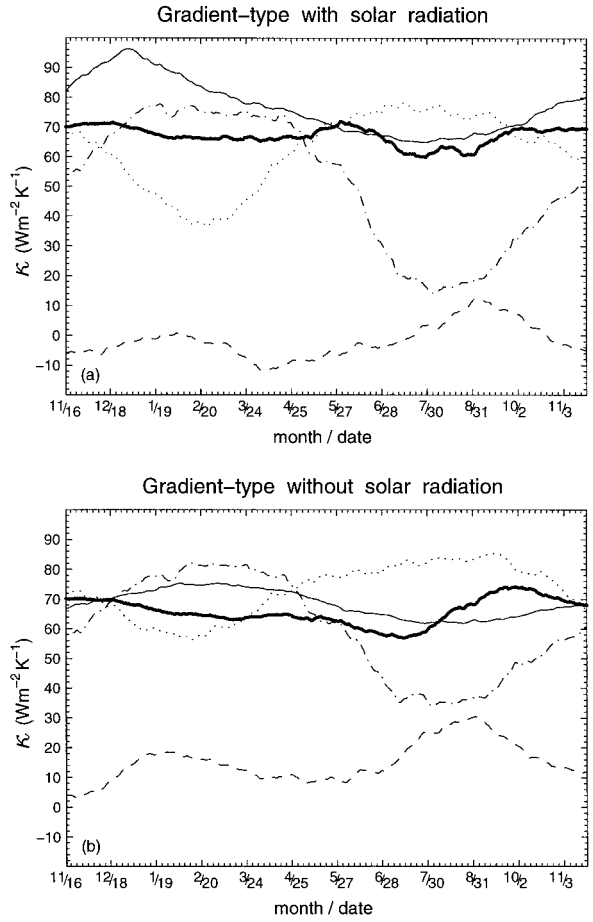


FIG. 6. Seasonal variation of coupling coefficient $\kappa$ averaged within five geographic zones determined by no loss of variance for (a) $Q = \kappa\Delta T_1$ and (b) $\tilde{Q} = \kappa\Delta T_1$. Here the thin solid curve indicates the southern middle and high latitude zone (south to 30°S), the thick solid curve indicates the northern middle and high latitude zone (north to 30°N), the dotted curve indicates the southern subtropical zone (10°–30°S), the dashed–dotted curve indicates the northern subtropical zone (10°–30°N), and the dashed curve indicates the equatorial zone (10°S–10°N).

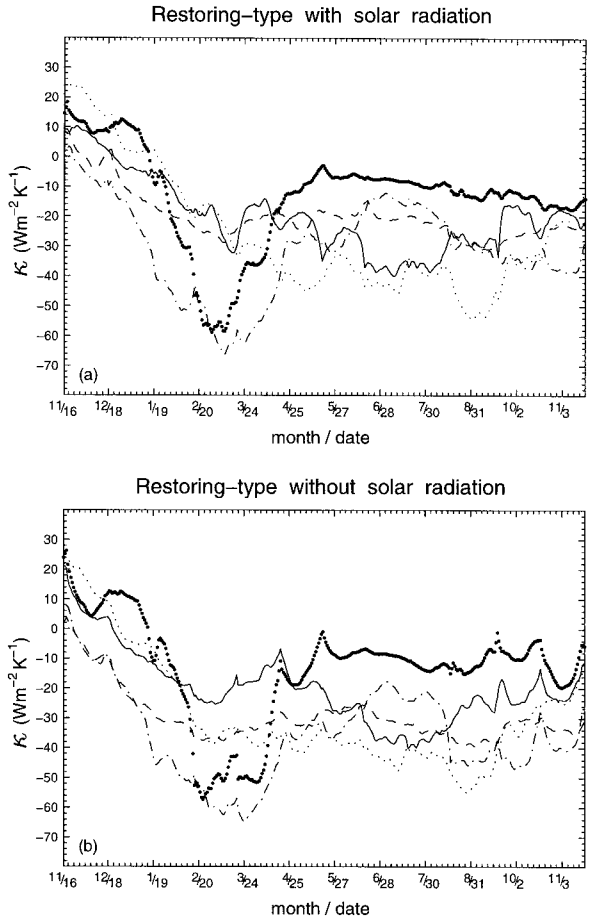


FIG. 7. Seasonal variation of coupling coefficient $\kappa$ averaged within five geographic zones determined by no loss of variance for (a) $Q = \kappa\Delta T_2$ and (b) $\tilde{Q} = \kappa\Delta T_2$. Here the thin solid curve indicates the southern middle and high latitude zone (south to 30°S), the thick solid curve indicates the northern middle and high latitude zone (north to 30°N), the dotted curve indicates the southern subtropical zone (10°–30°S), the dashed–dotted curve indicates the northern subtropical zone (10°–30°N), and the dashed curve indicates the equatorial zone (10°S–10°N).

tween $Q$ and $\Delta T_1$), from 0.22 to 0.54 in the southern subtropical zone, and from 0.1 to 0.54 in the northern subtropical zone (weak correlation between $Q$ and $\Delta T_1$). However, the value fluctuates from 0.7 to 0.86 all year round in the southern middle and high latitude zone (high correlation), and from 0.5 to 0.7 in the summer half-year (23 March–1 October) and from 0.7 to 0.86 in the winter half-year (1 October–23 March) in the northern middle and high latitude zone. On the basis of correlation, the surface thermal boundary condition, $Q = \kappa\Delta T_1$, is valid only in the middle and high latitudes. The cross-correlation coefficient $\overline{R}^{S}_{Q,\Delta T_1}(d)$ has seasonal variation in both northern and southern middle and high latitude zones: higher values during winter and lower values during summer. This may be caused by improper representation of the solar radiation $R_S$ by the temperature difference $\Delta T_1$.

#### 2) WITHOUT SOLAR RADIATION

Figure 4b illustrates the seasonal variation of $\overline{R}^{S}_{\tilde{Q},\Delta T_1}(d)$ for the five geographic zones. The correlation is higher between $\tilde{Q}$ and $\Delta T_1$ than between $Q$ and $\Delta T_1$, indicating the benefit of excluding the solar radiation from the net surface heat flux. For example, $\overline{R}^{S}_{\tilde{Q},\Delta T_1}(d)$ is near 0.86 year round in the southern middle and high latitudes, and varies between 0.74 and 0.84 in the northern middle and high latitudes. However, $\overline{R}^{S}_{\tilde{Q},\Delta T_1}(d)$ is still very low (between 0 and 0.2) in the equatorial zone and becomes higher but less than 0.7 in both northern and southern subtropical zones.

### *b. Restoring-type conditions*

Figure 5 illustrates the seasonal variations of $\overline{R}^{S}_{Q,\Delta T_1}(d)$ and $\overline{R}^{S}_{\tilde{Q},\Delta T_1}(d)$ for the five geographic zones, respectively.

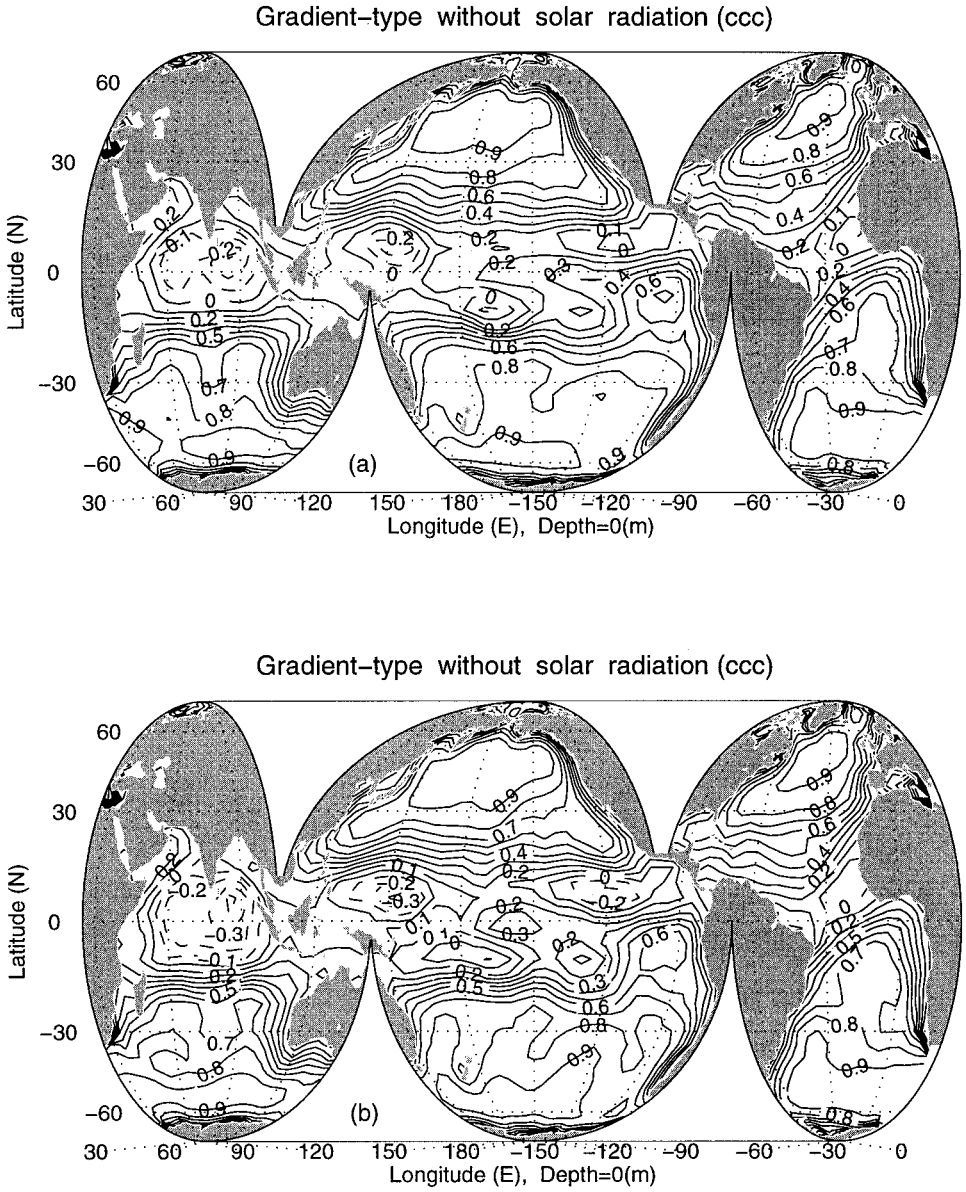


FIG. 8. Ensemble mean cross-correlation coefficients between $\Delta T_1$ and net surface heat flux without solar radiation $\tilde{Q}$ after the daily NCEP dataset undergoes (a) 30-day running mean, (b) 60-day running mean, and (c) 90-day running mean.

No matter where and when it is, there is no correlation between ($Q$, $\tilde{Q}$) and $\Delta T_2$ in the world oceans.

## 6. Seasonal variation of coupling coefficient $\kappa$

We computed the coupling coefficient $\kappa$ using (11) and then averaged $\kappa$ spatially within each of the five zones. Thus, we obtained both the spatial (five zones) and the temporal variability of $\kappa$. Theoretically, $\kappa$ can be time dependent. Practically, $\kappa$ is usually taken as a constant in the surface thermal boundary conditions (3), (4), (6), and (7). Therefore, besides high cross correlations, we should also consider quasi-steadiness of $\kappa$ in evaluating the surface thermal boundary conditions.

### *a. Gradient type*

For surface net heat flux with solar radiation (Fig. 6a), $\kappa$ varies from $-10$ to 10 W m$^{-2}$ K$^{-1}$ in the equatorial zone, from 15 to 78 W m$^{-2}$ K$^{-1}$ in the southern subtropical zone, from 36 to 80 W m$^{-2}$ K$^{-1}$ in the northern subtropical zone, from 70 to 95 W m$^{-2}$ K$^{-1}$ in the southern middle and high latitude zone, and from 60 to 70 W m$^{-2}$ K$^{-1}$ in the northern middle and high latitude

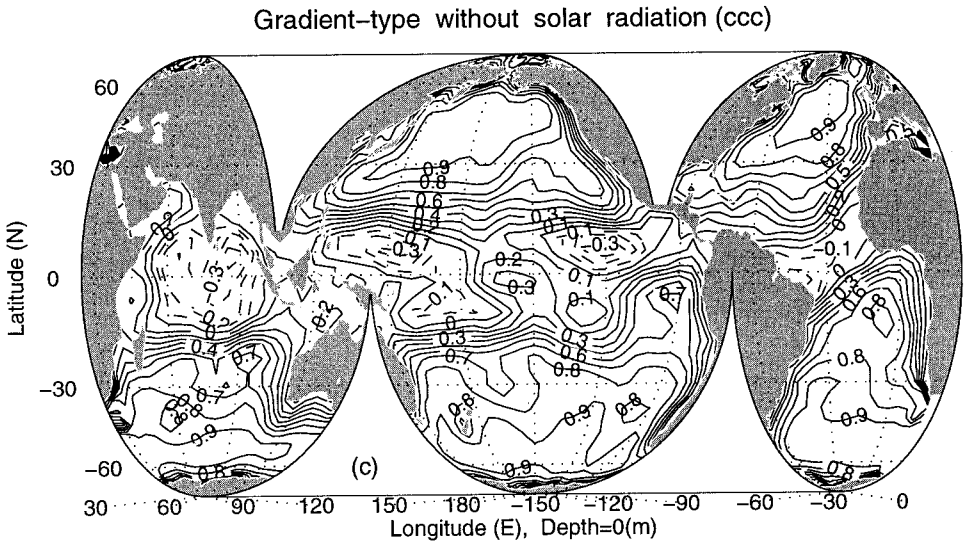


FIG. 8. (*Continued*)

zone. When the solar radiation is excluded from the net surface heat flux (Fig. 6b), $\kappa$ has large temporal variation in the equatorial zone. However, $\kappa$ has small temporal variation (56–74 W m$^{-2}$ K$^{-1}$) in the middle and high latitudes of both Northern and Southern Hemispheres.

On the basis of (i) high correlation between $\tilde{Q}$ and $\Delta T_1$, and (ii) quasi-steadiness of $\kappa$, we may conclude that the surface thermal boundary condition

$$\tilde{Q} = \kappa \Delta T_1$$

is a good parameterization of surface net heat flux for the middle and high latitudes.

### *b. Restoring type*

The coupling coefficient $\kappa$ has large spatial and temporal variation (from $-70$ to 25 W m$^{-2}$ K$^{-1}$) for both including and excluding solar radiation (Fig. 7). Several studies (Marotzke 1994; Rahmstorf and Willibrand 1995; Seager et al. 1995; Pierce et al. 1996; Marotzke and Pierce 1997) show the lengthscale dependence of values of $\kappa$ for the restoring-type boundary condition. For example, Seager et al. (1995) found that for typical anomaly length scales, a value of $\kappa$ of 15 W m$^{-2}$ K$^{-1}$ is appropriate.

Since (i) low correlation between ($Q$, $\tilde{Q}$) and $\Delta T_2$, and (ii) rapid variation of $\kappa$, we may conclude that the restoring-type conditions do not represent any surface thermal forcing and in turn any discussion on $\kappa$ for this type of condition is useless.

## 7. Timescale dependence of $\kappa$ for the gradient-type conditions

The coupling coefficient $\kappa$ has units of watts per square meter per kelvin. A timescale can be derived as $\tau = \rho c_p h/\kappa$, where $\rho$ is the density, $c_p$ is the specific heat of seawater, and $h$ is a typical mixed layer depth. Weaver and Sarachik (1991) used a timescale of 25 days. Marotzke and Willibrand (1991) used 30 days. For a mixed layer 50 m deep these correspond to values of $\kappa$ of 97 W m$^{-2}$ K$^{-1}$ and 81 W m$^{-2}$ K$^{-1}$, respectively. As pointed out by a number or authors (Zhang et al. 1993; Power et al. 1994; Santer et al. 1995; Rahmstorf and Willibrand 1995; Pierce et al. 1995; Cai and Chu 1996), change of values of $\kappa$ has detrimental effects on the realism of a modeled thermohaline circulation. Thus, use of a proper $\kappa$ value becomes an important issue. Section 6a shows that $\kappa$ varies from 60 to 76 W m$^{-2}$ K$^{-1}$ in the middle and high latitudes of both Northern and Southern Hemispheres based on the daily data. The gradient-type boundary conditions are used in ocean models when the variation is on different timescales. Many of them are on a seasonal timescale. In order to investigate the timescale dependence of $\kappa$ values, we use 30-day, 60-day, and 90-day running-mean operators on the original NCEP $R_S$, $R_b$, $Q_H$, $Q_E$, $T_O$, and $T_A$ to filter out high-frequency variations and obtain three datasets of global $Q(x, y, d)$, $\tilde{Q}(x, y, d)$, $T_A(x, y, d)$, and $T_O(x, y, d)$, respectively. The smoothed datasets have different durations: 16 October 1994–16 December 1995 for a 30-day smoothing, 31 October 1994–1 December 1995 for a 60-day smoothing, and 15 November 1994–16 November 1995 for a 90-day smoothing. For each smoothed dataset, we use (8) and (11) to compute CCC and between $Q$ and $\Delta T_1$ and the coupling coefficient for $Q = \kappa \Delta T_1$ at day $d$, which is computed in this paper from a 91-day subset between 45 days prior to and 45 days after that date.

The global distributions of $\langle R_{\tilde{Q},\Delta T_1} \rangle$ for the 30-day smoothed data (Fig. 8a), the 60-day smoothed data (Fig. 8b), and the 90-day smoothed data (Fig. 8c) show high

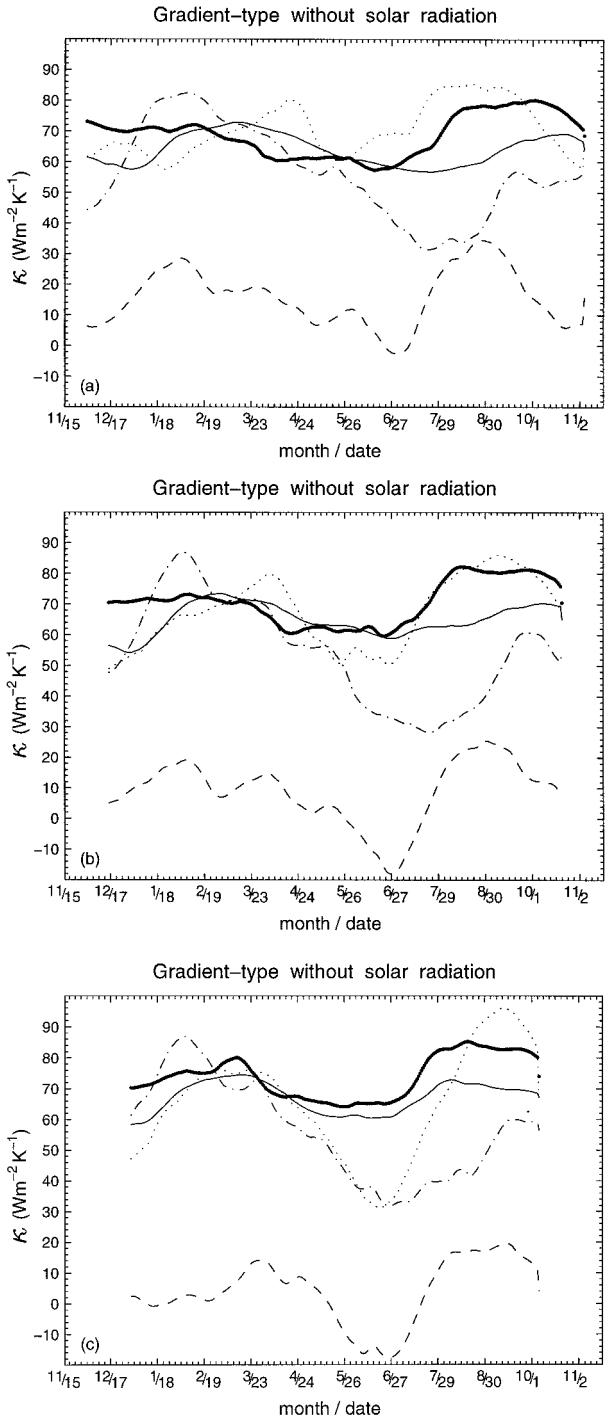


FIG. 9. Seasonal variation of coupling coefficient $\kappa$ averaged within five geographic zones, determined by no loss of variance for $\tilde{Q} = \kappa\Delta T_2$ after the daily NCEP dataset undergoes (a) 30-day running mean, (b) 60-day running mean, and (c) 90-day running mean. Here, the thin solid curve indicates the southern middle and high latitude zone (south to 30°S), the thick solid curve indicates the northern middle and high latitude zone (north to 30°N), the dotted curve indicates the southern subtropical zone (10°–30°S), the dashed–dotted curve indicates the northern subtropical zone (10°–30°N), and the dashed curve indicates the equatorial zone (10°S–10°N).

values of CCC in middle and high latitudes (higher than 30°) away from coasts, low values of CCC in equatorial regions (10°N–10°S), and not much difference in CCC among the three smoothed datasets. Comparison between Fig. 8 and Fig. 1b indicates the increase of CCC in middle and high latitudes from the unsmoothed data (~0.8) to the smoothed data (~0.9). Thus, the gradient-type Haney boundary condition is also valid in middle and high latitudes (higher than 30°) away from coasts and invalid in equatorial regions (10°N–10°S) for smoothed data. The validity is enhanced when the data is smoothed over 30 days or longer.

The coupling coefficient $\kappa$ between $\tilde{Q}$ and $\Delta T_1$ for the 30-day smoothed data (Fig. 9a), the 60-day smoothed data (Fig. 9b), and the 90-day smoothed data (Fig. 9c) has large seasonal variations in the equatorial and subtropical zones, and small seasonal variations in the middle and high latitude zones. This feature is very similar to the unsmoothed data. Comparison between Fig. 9 and Fig. 6b shows no drastic change of $\kappa$ from the unsmoothed daily dataset to three different (30-day, 60-day, and 90-day) smoothed datasets for both northern and southern middle and high latitude zones. We may use 70 W m$^{-2}$ K$^{-1}$ for the northern middle and high latitude zone and 65 W m$^{-2}$ K$^{-1}$ for the southern middle and high latitude zone.

## 8. Conclusions

Haney-type surface thermal boundary conditions connect net downward surface heat flux to air–sea temperature difference (gradient-type condition) or to climate/synoptic sea temperature difference (restoring-type condition). On the basis of cross-correlation and variance analyses on the NCEP net downward surface heat flux and air–sea temperature data during 1 October 1994–31 December 1995, we obtained the following results:

1) The restoring-type conditions do not represent the surface thermal forcing anywhere in the world oceans.
2) For the equatorial and subtropical oceans, the gradient-type conditions are not good approximations for the surface thermal forcing.
3) For the middle and high latitudes away from coasts, the gradient-type conditions are good approximation for the surface thermal forcing. This is based on the high correlation between net downward heat flux and air–sea temperature difference and associating quasi-steadiness of the coupling coefficient $\kappa$. Furthermore, there is a better correlation when the solar shortwave component is treated separately.
4) A value of 70 W m$^{-2}$ K$^{-1}$ (65 W m$^{-2}$ K$^{-1}$) for the coupling coefficient $\kappa$ is suggested for northern (southern) middle and high latitude zones, no matter whether the data is smoothed or unsmoothed. The suggested values are about twice those generally

used (10–50 W $m^{-2}$ $K^{-1}$). This might increase the net air–sea heat flux and shorten the relaxation time.

We also tried a coupled air–ocean model developed by Russell et al. (1995), and we found essentially similar results.

*Acknowledgments.* The authors are indebted to Roland H. Schweitzer at the University of Colorado at Boulder for providing the NCEP dataset. This work was funded by the Office of Naval Research NOMP Program.

## REFERENCES

Blumberg, A., and G., Mellor, 1987: A description of a three dimensional coastal ocean circulation model. *Three Dimensional Coastal Ocean Models,* N. S. Heaps, Ed., Amer. Geophys. Union, 1–16.

Cai, W. J., and P. C. Chu, 1996: Ocean climate drift and interdecadal oscillation due to a change in thermal damping. *J. Climate,* **9,** 2821–2833.

Cayan, D. R., 1992: Latent and sensible heat flux anomalies over the northern oceans: Driving the sea surface temperature. *J. Phys. Oceanogr.,* **22,** 859–881.

Han, Y. J., 1984: A numerical World Ocean general circulation model. Part II: A baroclinic experiment. *Dyn. Atmos. Oceans,* **8,** 141–172.

Haney, R. L., 1971: Surface thermal boundary condition for ocean circulation models. *J. Phys. Oceanogr.,* **1,** 241–248.

Marotzke, J., 1994: Ocean models in climate problems. *Ocean Processes in Climate Dynamics: Global and Mediterranean Examples,* P. Malanotte-Rizzoli and A. R. Robinson, Eds., Kluwer, 79–109.

——, and J. Willibrand, 1991: Multiple equilibria of global thermohaline circulation. *J. Phys. Oceanogr.,* **21,** 1372–1385.

——, and D. Pierce, 1997: On spatial scales and lifetimes of SST anomalies beneath a diffusive atmosphere. *J. Phys. Oceanogr.,* **27,** 133–139.

Oberhuber, J. M., 1988: An atlas based on the COADS data set: The budgets of heat, buoyancy and turbulent kinetic energy at the surface of the global ocean. Tech. Rep. 15, Max-Planck-Institut für Meteorologie, Hamburg, Germany, 199 pp.

Pierce, D., 1996: Reducing phase and amplitude errors in restoring boundary conditions. *J. Phys. Oceanogr.,* **26,** 1552–1560.

——, T. P. Barnett, and U. Mikolajewicz, 1995: Competing roles of heat and freshwater flux in forcing thermohaline oscillations. *J. Phys. Oceanogr.,* **25,** 2046–2064.

Power, S. B., A. M. Moore, D. A. Post, N. R. Smith, and R. Kleeman, 1994: Stability of North Atlantic Deep Water formation in a global ocean general circulation model. *J. Phys. Oceanogr.,* **24,** 904–916.

Rahmstorf, S., and J. Willebrand, 1995: The role of temperature feedback stabilizing the thermohaline circulation. *J. Phys. Oceanogr.,* **25,** 787–805.

Russell, G. L., J. R. Miller, and D. Rind, 1995: A coupled atmosphere–ocean model for transient climate change studies. *Atmos.-Ocean,* **33,** 683–730.

Santer, B. D., U. Mikolajewicz, W. Bruggemann, U. Cubasch, K. Hasselmann, H. Hock, E. Marier-Reimer, and T. M. L. Wigley, 1995: Ocean variability and its influence on the detectability of greenhouse warming signals. *J. Geophys. Res.,* **100,** 10 693–10 725.

Seager, R., Y. Kushnir, and M. A. Cane, 1995: On heat flux boundary conditions for ocean models. *J. Phys. Oceanogr.,* **25,** 3219–3230.

Weaver, A. J., and E. S. Sarachik, 1991: Evidence for decadal variability in an ocean general circulation model: An advective mechanism. *Atmos.–Ocean,* **29,** 197–231.

Zhang, S., R. J. Greatbatch, and C. A. Lin, 1993: A reexamination of the polar halocline catastrophe and implications for coupled ocean–atmosphere modeling. *J. Phys. Oceanogr.,* **23,** 287–299.